Catena 221 (2023) 106745

Contents lists available at ScienceDirect

Catena

journal homepage: www.elsevier.com/locate/catena

Scale-specific variation in daily suspended sediment load in karst catchments

Zhenwei Li, Xianli Xu *, Kelin Wang

Huanjiang Observation and Research Station for Karst Ecosystem, Key Laboratory for Agro-Ecological Processes in Subtropical Region, Institute of Subtropical Agriculture, Chinese Academy of Sciences, Changsha 410125, China
Guangxi Key Laboratory of Karst Ecological Processes and Services, Huanjiang 547100, China
Institutional Center for Shared Technologies and Facilities of Institute of Subtropical Agriculture, Chinese Academy of Sciences, Changsha 410125, China

ARTICLE INFO

Keywords:
Soil erosion
Nonlinear and nonstationary
Multiscale correlations
Multivariate empirical mode decomposition
Ecohydrology

ABSTRACT

Temporal variation in sediment load is generally scale dependent and affected by many factors operating at different timescales. Due to the complexity of sediment transportation mechanisms and the nonlinear behavior of hydrological processes, identifying multi-timescale effects of variables on daily suspended sediment load (SSL) is challenging. Using multivariate empirical mode decomposition (MEMD), the aims of this study were to investigate scale-dependent relationships between daily SSL and associated variables and to predict daily SSL based on these relationships. Data on daily SSL in four typical karst catchments of southwest China and five potential variables affecting daily SSL (i.e., runoff, precipitation, air temperature, potential evapotranspiration, and Normalized Differential Vegetation Index) were collected during 2009–2012. The results indicated that MEMD decomposed temporal patterns of daily SSL and five potential variables affecting daily SSL into eight or nine intrinsic mode functions (IMFs) and a residue. Short timescale oscillations of IMF1 to IMF4 contributed more than 72 % of the total variance in daily SSL in the four catchments, indicating that temporal variation in SSL was dominated by short intervals of 4–23 days. Runoff was the dominant explanatory variable for the overall daily suspended sediment load prediction at the observation scale. The predictions of daily SSL based on the IMFs and their residuals greatly outperformed those based on the original time series data. This result implies that a single scale (e.g., observation scale) is not sufficient to capture the complex relationships that exist between daily SSL and associated variables at all timescales. The results demonstrate the superiority of MEMD in characterizing scale-specific relationships between daily SSL and associated variables and improving daily SSL predictions. Given the complexity, nonlinearity, and nonstationarity inherent in many hydrological and sediment transport processes, MEMD is recommended for identifying scale-specific variation in daily SSL in future studies.

1. Introduction

Sediment transport is a complex hydrological and environmental phenomenon, which greatly influenced various factors, including water quality, channel navigability, hydroelectric equipment longevity, fish and invertebrate habitat, and river restoration (Syvitski et al., 2005; Wang et al., 2016; Li et al., 2020a). In the past, sediment transport during rainstorms or floods has had catastrophic consequences for humans and built infrastructure (Borrelli et al., 2020; Liu et al., 2020). Sediment transport processes show a high degree of temporal variability due to the nonlinear physical factors, including rainfall, that govern them. (Ma et al., 2010; Cook et al., 2015; Rice et al., 2016; Vercruysse et al., 2017; Sok et al., 2021). A better understanding of suspended sediment load (SSL) transportation mechanisms, in addition to potential variables affecting SSL, is important to control sediment delivery and to manage river flows effectively.

SSL is generally closely related to hydrological processes, climate variability, and vegetation dynamics (de Vente et al., 2013; Li et al., 2016; Vercruysse et al., 2017). Runoff is usually the main driver of eroded sediment in rivers and thus exerts a substantial influence on SSL (Wang et al., 2016; Li et al., 2020c). Climatic indices, such as precipitation, temperature, and potential evapotranspiration (PE), also exert a major influence on SSL (Li et al., 2017b; Zhang, 2020). Generally, the SSL increases in accordance with an increase in precipitation (Borrelli

* Corresponding author at: Huanjiang Observation and Research Station for Karst Ecosystem, Key Laboratory for Agro-Ecological Processes in Subtropical Region, Institute of Subtropical Agriculture, Chinese Academy of Sciences, Changsha 410125, China.
E-mail addresses: lizhenwei337@isa.ac.cn (Z. Li), xianlixu@isa.ac.cn (X. Xu), kelin@isa.ac.cn (K. Wang).

https://doi.org/10.1016/j.catena.2022.106745
Received 13 June 2022; Received in revised form 24 October 2022; Accepted 26 October 2022
Available online 12 November 2022

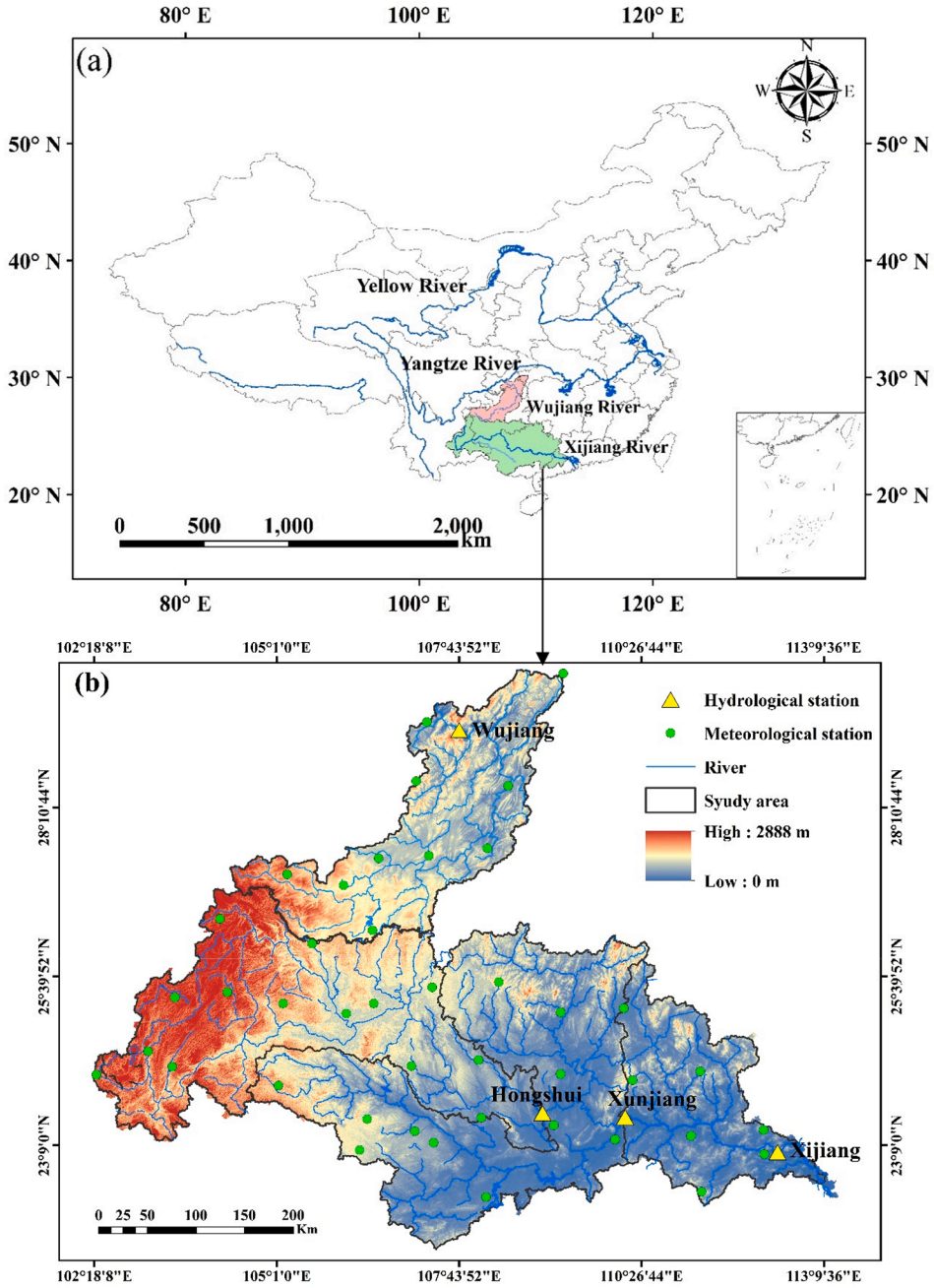

Fig. 1. Locations of the (a) study catchments, (b) meteorological stations, hydrological stations, and DEM.

et al., 2020; Zheng et al., 2021). Temperature and PE are closely associated with runoff and plant growth and indirectly affect sediment load (Zhang, 2020; Li et al., 2021). Vegetation can decrease raindrop kinetic energy, improve soil properties, delay the initial runoff yielding time, and hence influence sediment production, transport, and delivery in rivers (Knapen et al., 2007; Shi et al., 2013; Duan et al., 2016).

Due to the nonlinear and nonstationary nature of river flows, the relationships between SSL and potential SSL-related variables are complex and timescale dependent (Gao et al., 2016; Rice et al., 2016). As a result, a variable that exerts a strong effect on SSL at one timescale may exert only a weak effect at another timescale. The specific scale of the dominant driver of SSL may change, depending on the measurement scale (e.g., daily, weekly, monthly). Consequently, it is essential to identify relationships between SSL and variables potentially affecting SSL at multiple timescales.

Spectral analysis, temporal coherency, and wavelet analysis are generally used to evaluate scale-dependent relationships between SSL and potential variables influencing SSL (Zhang et al., 2009; Gao et al., 2016). However, both spectral analysis and temporal coherency require linearity and stationarity of time series to be managed, and therefore it is difficult to satisfy the sediment transport processes (Si, 2008; Yang et al., 2019a). Although wavelet analysis can handle nonstationary data, it is useful only for exploring temporal correlations between two variables at different timescales (Yang et al., 2022). Evaluating the influence of one variable is likely inadequate to represent the intricate and complex nature of the sediment transport process. Recently, multivariate empirical mode decomposition (MEMD), an extension of univariate empirical mode decomposition, was shown to cope well with nonlinear and nonstationary signals (Rehman and Mandic, 2010). MEMD can decompose multiple variables into a group of intrinsic oscillatory modes or intrinsic mode functions (IMFs) and a residue to investigate scale-dependent relationships (Hu and Si, 2013). In this way, MEMD can

identify the true scale at which underlying processes influence SSL. Due to the advantages of MEMD, it has been widely used to characterize scale-specific controls of soil moisture, soil hydraulic conductivity, soil water infiltration, soil water repellency, and soil erodibility (Hu and Si, 2013; Hu et al., 2014; She et al., 2014; She et al., 2017; Zhao et al., 2017; Liu et al., 2018b; Liu et al., 2019; Yang et al., 2019a; Zhu et al., 2021; Yang et al., 2022). However, few studies have used MEMD to quantify scale-dependent relationships of SSL and factors affecting SSL, especially in karst watersheds subject to severe soil erosion and more complex sediment transport processes than those in non-karst regions.

The karst region of southwest China is one of the largest in the world. The region is characterized by shallow soil layers, scattered rock outcrops, unique hydrogeological conditions, complex geomorphology, fragmented landscapes, and rich biodiversity (Hartmann et al., 2014; Tong et al., 2018; Wang et al., 2019). As the highly soluble carbonate rocks in the region produce little soil, the soil formation rate is very low (Peng and Wang, 2012; Li et al., 2019; Cao et al., 2020b). Furthermore, once soil that has formed is lost, recovery of the soil layer is difficult, as a period of several thousands of years is required to produce 1 cm of soil in pure carbonate rocks (Jiang et al., 2014; Cao et al., 2020a). Dissolution of carbonate rocks can also lead to the formation of complex voids composed of fractures, fissures, caves and conduits, all of which contribute to freshwater movement and storage (Wilcox et al., 2008; Dai et al., 2017). As a result, a small number of large rainfall erosion events usually drive sediment load variation at the annual scale in karst regions (Cao et al., 2020a; Li et al., 2020c). Thus, SSL in karst regions exhibits high temporal variability, especially at the daily scale.

Although data on daily runoff are generally available, data on SSL are usually collected at weekly or monthly scales. Thus, it is extremely challenging to clarify the complex and nonlinear interactions between daily SSL and potential SSL-related variables at a wide range of temporal scales. The objectives of the current study were: (1) to characterize scale-specific temporal variation in daily SSL in four typical karst catchments during 2009–2012 using the MEMD method, (2) to identify scale-dependent interactions between daily SSL and SSL-related variables at different timescales, and (3) to estimate the daily SSL at the scale of observation based on the multiscale relationships examined in (2).

2. Study area and data

2.1. Study area

This study was conducted in Wujiang (26°09′–30°12′N; 104°15′–109°20′E) and Xijiang (102°16′–113°23′E, 21°36′–27°00′N) catchments, a typical karst region in southwest China (Fig. 1a). Wujiang catchment has a drainage area of 8.8×10^4 km^2, with elevation ranging from 113 m in the southeast to 2,888 m in the northwest (Fig. 1b). The Wujiang River is the largest southern tributary of the upper reaches of the Yangtze River, and its main stream is 1,037 km long. Wujiang River originates in the Wumeng Mountains in western Guizhou Province, then runs through three provinces (Yunnan, Chongqing, and Hubei) and finally flows into the Yangtze River. Wujiang catchment has a subtropical monsoon humid climate, with an average annual temperature of 12 °C and annual precipitation ranging from 1,100 to 1,300 mm. The distribution of precipitation is nonuniform throughout the year, with greater than 70 % occurring between May and September. The average annual runoff and sediment yield in Wujiang catchment during 1955–2015 were 552 mm and 273 t km^{-2}, respectively. Xijiang River is the largest tributary of Pearl River, with a main stream length of 2,214 km and a drainage area of 3.53×10^5 km^2. It is sourced from the Yunnan–Guizhou plateau and empties into the South China Sea through Yunnan, Guizhou, Guangxi, and Guangdong Provinces. Xijiang catchment has a subtropical climate, with an annual mean temperature of 14–22 °C and precipitation of 1,200–2000 mm. Approximately 80 % of precipitation falls during the rainy season (April – October). The average annual runoff and sediment yield in Xijiang catchment during 1955–2015 were 650 mm and 184 t km^{-2}, respectively.

Two other catchments, Hongshui and Xunjiang, which are located within Xijiang catchment, were also selected as study sites (Fig. 1b). Karst landscapes are widespread in the study area, with rock matrix, fractures, conduits, curved channels, underground streams, karst caves, and sinkholes extensively distributed. Exposed karst areas account for about 77 % and 44 % of the surface in Wujiang and Xijiang catchments, respectively. Fig. 1 shows the locations of the meteorological and hydrological stations in the study area.

2.2. Data

Daily runoff, SSL, precipitation, air temperature, PE, and Normalized Difference Vegetation Index (NDVI) were the variables evaluated in the present study. Data on daily runoff (m^3/s) and SSL (kg s^{-1}) for Wujiang, Xijiang, Hongshui, and Xunjiang catchments during 2009–2012 were obtained from the Ministry of Water Resources of China. The homogeneity and reliability of the dataset were examined and strictly controlled before its release. Continuous data on daily runoff and SSL were available in Wujiang catchment for 2009–2012. Daily runoff and SSL records for Xijiang and Xunjiang catchments were missing for the following periods: 3 September to 5 September 2010, 14 March to 15 March 2011, 3 February to 27 February 2012, and 15 December 2012. Data on daily runoff and SSL were also missing in Hongshui catchment for 3 September to 5 September 2010, 14 March to 15 March 2011, and 15 December 2012. Daily precipitation and air temperature data from meteorological stations were obtained from the China Meteorological Administration. PE was calculated using the modified Penman formula (Mccoll, 2020). Catchment-based daily precipitation, air temperature, and PE were calculated using the CoKriging interpolation method in ArcGIS. The daily NDVI was derived from the National Oceanic and Atmospheric Administration/Advanced Very High Resolution Radiometer (NOAA/AVHRR) surface reflectance product [https://code.earthengine.google.com/]. The DEM with a resolution of 30 m × 30 m was downloaded from the Geospatial Data Cloud and used to extract the boundary of each catchment using ArcGIS software.

3. Methodology

3.1. Trend test

The Mann-Kendall (M–K) nonparametric test was applied to detect temporal trends in daily precipitation, runoff, and SSL in the four selected karst catchments (Mann, 1945; Kendall Maurice, 1975). This test is unaffected by individual outliers, and samples can be randomly distributed. For a given time series X (X_1, X_2, …, X_n), the test statistic S value and the standard statistic Z value were:

$$S = \sum_{i=1}^{n-1} \sum_{j=i+1}^{n} \operatorname{sgn}(x_j - x_i) \tag{1}$$

$$\operatorname{sgn}(x_j - x_i) = \begin{cases} 1 & x_j > x_i \\ 0 & x_j = x_i \\ -1 & x_j < x_i \end{cases} \tag{2}$$

$$Var(S) = \frac{n(n-1)(2n+5) - \sum_{p=1}^{q} t_p (t_p - 1)(2t_p + 5)}{18} \tag{3}$$

Table 1
Descriptive statistics of daily suspended sediment load (SSL) and five potential variables affecting daily SSL in four karst catchments.

Catchment	Variables	Min	Max	Mean	SD	CV (%)	*n*
Wujiang	Sediment load (kg s^{-1})	1.0	22,720	77.3	678	877	1,461
	Runoff (m^3/s)	312	14,200	1,248	1,031	83	1,461
	Precipitation (mm)	0.0	54.0	2.7	5.5	207	1,461
	Temperature (℃)	−2.0	28.4	15.2	7.8	51	1,461
	PE (mm)	0.6	6.6	2.4	1.4	56	1,461
	NDVI (%)	−3.3	60.1	11.1	12.6	113	1,461
Xijiang	Sediment load (kg s^{-1})	1.7	22,188	453.2	1,488	328	1,430
	Runoff (m^3/s)	644	35,500	5668	5,077	90	1,430
	Precipitation (mm)	0.0	50.1	3.5	5.4	156	1,430
	Temperature (℃)	2.4	28.9	19	6.5	34	1,430
	PE (mm)	0.9	6.2	2.9	1.2	40	1,430
	NDVI (%)	−0.7	56.3	15.5	11.6	75	1,430
Hongshui	Sediment load (kg s^{-1})	0.5	773	15.7	47.9	306	1,455
	Runoff (m^3/s)	221	7,010	1,514	950	63	1,455
	Precipitation (mm)	0.0	69.6	2.9	5.7	195	1,455
	Temperature (℃)	1.2	26.9	17.2	6.3	37	1,455
	PE (mm)	0.8	6.9	2.8	1.2	42	1,455
	NDVI (%)	−2.1	55.8	15.5	11.5	74	1,455
Xunjiang	Sediment load (kg s^{-1})	1.9	24,290	290	1,164	401	1,430
	Runoff (m^3/s)	802	34,900	4,475	3,883	87	1,430
	Precipitation (mm)	0.0	51.2	3.2	5.4	169	1,430
	Temperature (℃)	1.8	28.3	18.4	6.5	35	1,430
	PE (mm)	0.8	6.4	2.9	1.2	41	1,430
	NDVI (%)	−1.6	56.3	15.4	11.7	76	1,430

PE: potential evapotranspiration; NDVI: normalized differential vegetation index; SD: standard deviation; CV: coefficient of variation; *n*: number of samples.

$$Z=\begin{cases}(S-1)\Big/\sqrt{Var(S)} & S>0\\ 0 & S=0\\ (S+1)\Big/\sqrt{Var(S)} & S<0\end{cases} \tag{4}$$

where n is the time series; x_i and x_j are data values in chronological order ($j>i$); S and Z are the test and standard statistics, respectively; q is the number of tied values; and t_p is the number of ties for the pth value. This method tests the original hypothesis by constructing parameter Z at the α significance level. If $|Z|>Z_{(1-\alpha/2)}$, there is an increasing or decreasing time series trend. A significance level of $\alpha=5$ % was selected in the present study. A positive/negative Z value indicated an increasing/decreasing trend. The effect of serial correlation on the M−K test was removed using the trend-free pre-whitening method at the 0.05 significance level. The M−K trend analysis was applied in MATLAB R2020a software.

3.2. Memd

To shed light on the dominant factors influencing daily SSL at different temporal scales, the MEMD method was applied to decompose temporal patterns of daily SSL and associated variables (runoff, precipitation, air temperature, PE, and NDVI) into different IMFs plus a residue term. Considering the n time series $X(t)=\{x_1(t),\ x_2(t),\ldots,x_n(t)\}$ as a function of time (t), nonstationary and nonlinear n-dimensional data sets were calculated by MEMD as follows (Rehman and Mandic, 2010; Hu et al., 2014):

(i) Create a set of angles $\theta^k=\left\{\theta_1^k,\ \theta_2^k,\ldots,\theta_{n-1}^k\right\}(k=1,2,\ldots,d$, where d is the total number of direction in a direction set, and then generate a suitable set of direction vectors of $V^{\theta_k}=\{v_1^k,\ v_2^k,\ldots,v_n^k\}$ using these angles;

(ii) Compute the projection, denoted by$p^{\theta_k}(t)$, of the time series $X(t)$ along the set of direction vectors$v_1^k,\ v_2^k,\ldots,v_n^k$, for all the k;

(iii) Search the temporal instants $t_i^{\theta_k}$ corresponding to the maxima of $p^{\theta_k}(t)$ for all the k;

(iv) Interpolate the $\left[t_i^{\theta_k},\ X(t_i^{\theta_k})\right]$ to acquire multivariate envelope curves,$e^{\theta_k}(t)$, for all the k;

(v) Calculate the average $M(t)$ of the envelope curves using $M(t)=1/d\sum_{k=1}^{d}e^{\theta_k}(t)$ for the time series, $X(t)$;

(vi) Subtract the "specific'' $C(t)$ using $C(t)=X(t)$–$M(t)$. If "specific'' $C(t)$ meets the stoppage criterion for a multivariate IMF, execute the procedure above on $X(t)$–$C(t)$. Otherwise, run the steps on $C(t)$.

After decomposition of the variables, the Hilbert transformation was carried out to obtain the instantaneous frequency of each IMF (Huang et al., 1998). Subsequently, the instantaneous frequencies of daily SSL and associated variables were transformed to period (1/frequency). The period and variance contributions for each IMF were then calculated. Detailed information on the MEMD procedure is available elsewhere (Rehman and Mandic, 2010, 2011; Looney et al., 2015). The MEMD and Hilbert transform codes were provided by Rehman and Mandic (2009) and Rilling (2007), respectively, and were both operated in MATLAB R2020a software.

3.3. Statistical analysis

Pearson's correlation analysis was used to quantify the relationships between the IMF or the residue of daily SSL and the five SSL-related variables. The stepwise multiple linear regression (MLR) method was used to estimate the daily SSL or residue at each scale using the runoff, precipitation, air temperature, PE, and NDVI from the corresponding IMF or residue. The predicted daily SSL at the observation scale was then calculated by adding all the predicted values for each IMF and residue of daily SSL. Pearson's correlation analysis and stepwise MLR were implemented using SPSS 22.0 software.

Daily SSL predictions were evaluated by the coefficient of determination (R^2), Akanke's Information Criterion (*AIC*), and root mean squared error (*RMSE*). The R^2, *AIC*, and *RMSE* were calculated by the following equations:

$$R^2=\frac{\left[\sum_{i=1}^{n}(Pi-Pm)(Oi-Om)\right]^2}{\sum_{i=1}^{n}(Pi-Pm)^2(Oi-Om)^2} \tag{5}$$

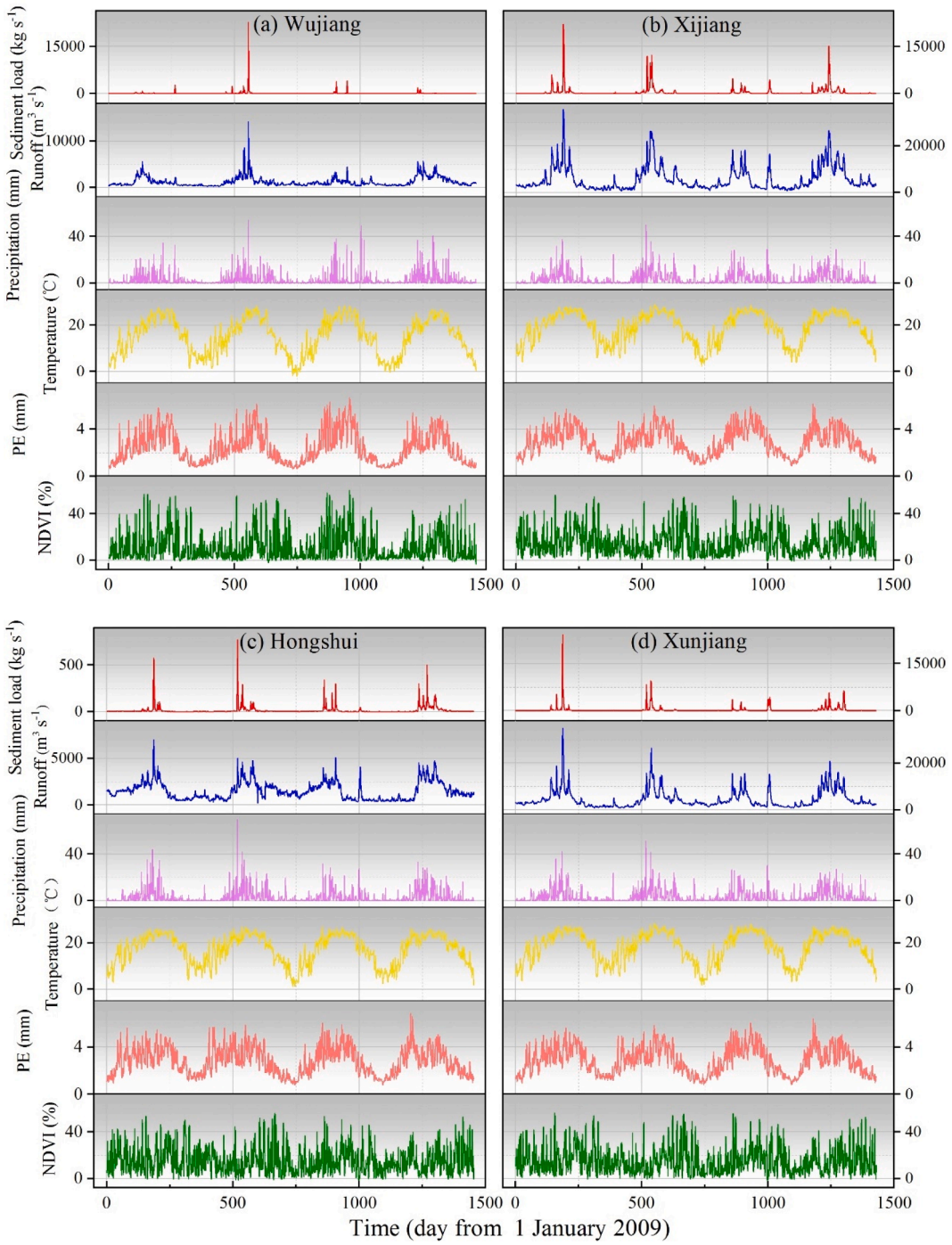

Fig. 2. Temporal variation in daily suspended sediment load (SSL), runoff, precipitation, air temperature, potential evapotranspiration (PE), and normalized differential vegetation index (NDVI) values at (a) Wujiang, (b) Xijiang, (c) Hongshui, and (d) Xujiang karst catchments from 1 January 2009 to 31 December 2012.

$$AIC = \ln\left[\frac{1}{n}\sum_{i=1}^{n}(Oi - Pi)^2\right] + \frac{2h}{n} \quad (6)$$

$$RMSE = \sqrt{\frac{1}{n}\sum_{i=1}^{n}(O_i - P_i)^2} \quad (7)$$

where P_i and O_i are the predicted and observed daily SSL values, respectively; n is the total number of variables; P_m and O_m are the mean values of the predicted and observed daily SSL values, respectively; h is the number of regression variables. The model showed the best goodness of fit when the *AIC* and *RMSE* values were the lowest and when the R^2 was as close as possible to 1.

4. Results and discussion

4.1. Temporal variation in daily SSL and associated variables

Table 1 presents the statistical data on daily SSL and five potential SSL-related variables. The minimum daily SSL was almost the same in the four karst catchments. The maximum value in Hongshui catchment was one thirtieth of the value in the other three catchments. Similarly, the mean daily SSL in Hongshui catchment was 15.7 kg s^{-1}, which was much lower than that in Wujiang, Xijiang, and Xunjiang catchments. In

Table 2
Summary of the trend analysis of daily suspended sediment load (SSL), runoff, and precipitation using the Mann-Kendall (M−K) test.

	Wujiang Sediment load (kg s^{-1})	Runoff (m^3/s)	Precipitation (mm)	Xijiang Sediment load (kg s^{-1})	Runoff (m^3/s)	Precipitation (mm)	Hongshui Sediment load (kg s^{-1})	Runoff (m^3/s)	Precipitation (mm)	Xunjiang Sediment load (kg s^{-1})	Runoff (m^3/s)	Precipitation (mm)
S	-6×10^5	3×10^5	9×10^4	-3×10^5	3×10^5	8×10^5	6×10^5	1×10^5	7×10^4	4×10^5	2×10^5	7×10^4
Z	−34	18	5	−17	14	4	32	−7	4	23	13	1
P	< 0.01	< 0.01	< 0.01	< 0.01	< 0.01	< 0.01	< 0.01	< 0.01	< 0.01	< 0.01	< 0.01	< 0.01
Trend	↓	↑	↑	↓	↑	↑	↑	↓	↑	↑	↑	↑

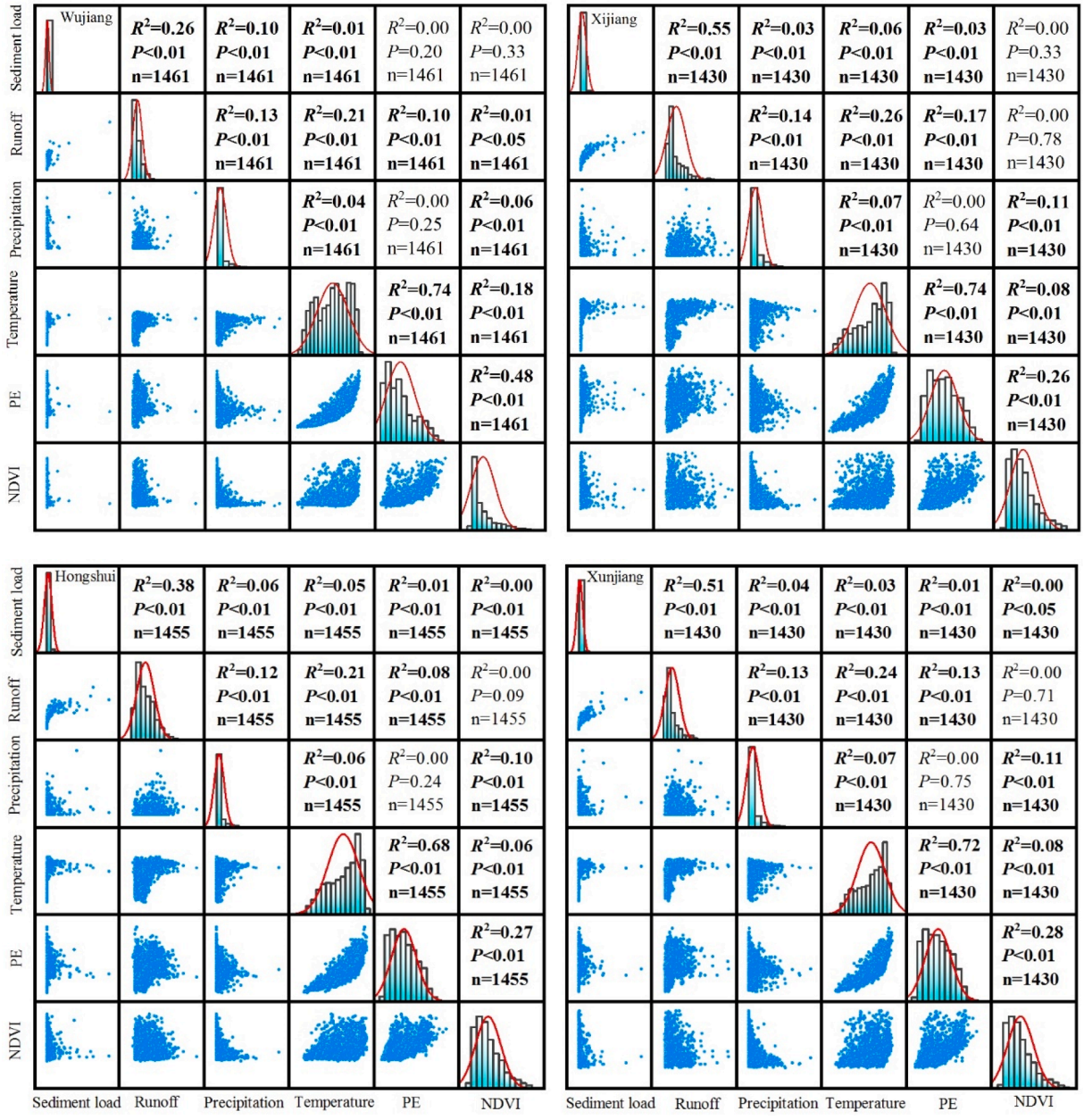

Fig. 3. Bivariate scatterplot matrix of daily suspended sediment load (SSL), runoff, precipitation, air temperature, potential evapotranspiration (PE), and normalized differential vegetation index (NDVI) values at Wujiang, Xijiang, Hongshui, and Xujiang karst catchments. Numbers in bold denote $P < 0.05$ or $P < 0.01$.

all four catchments, the coefficient of variation (CV) for daily SSL showed strong variability, with values ranging from 306 % to 877 %, which was much larger than the CV of the five potential variables influencing daily SSL. Temporal variation in sediment transport is nonstationary and nonlinear and is markedly affected by both intrinsic and extrinsic factors, such as soil properties, climactic variables, and plant characteristics, leading to substantial variability in daily SSL (Knapen et al., 2007; de Vente et al., 2013; Vercruysse et al., 2017;

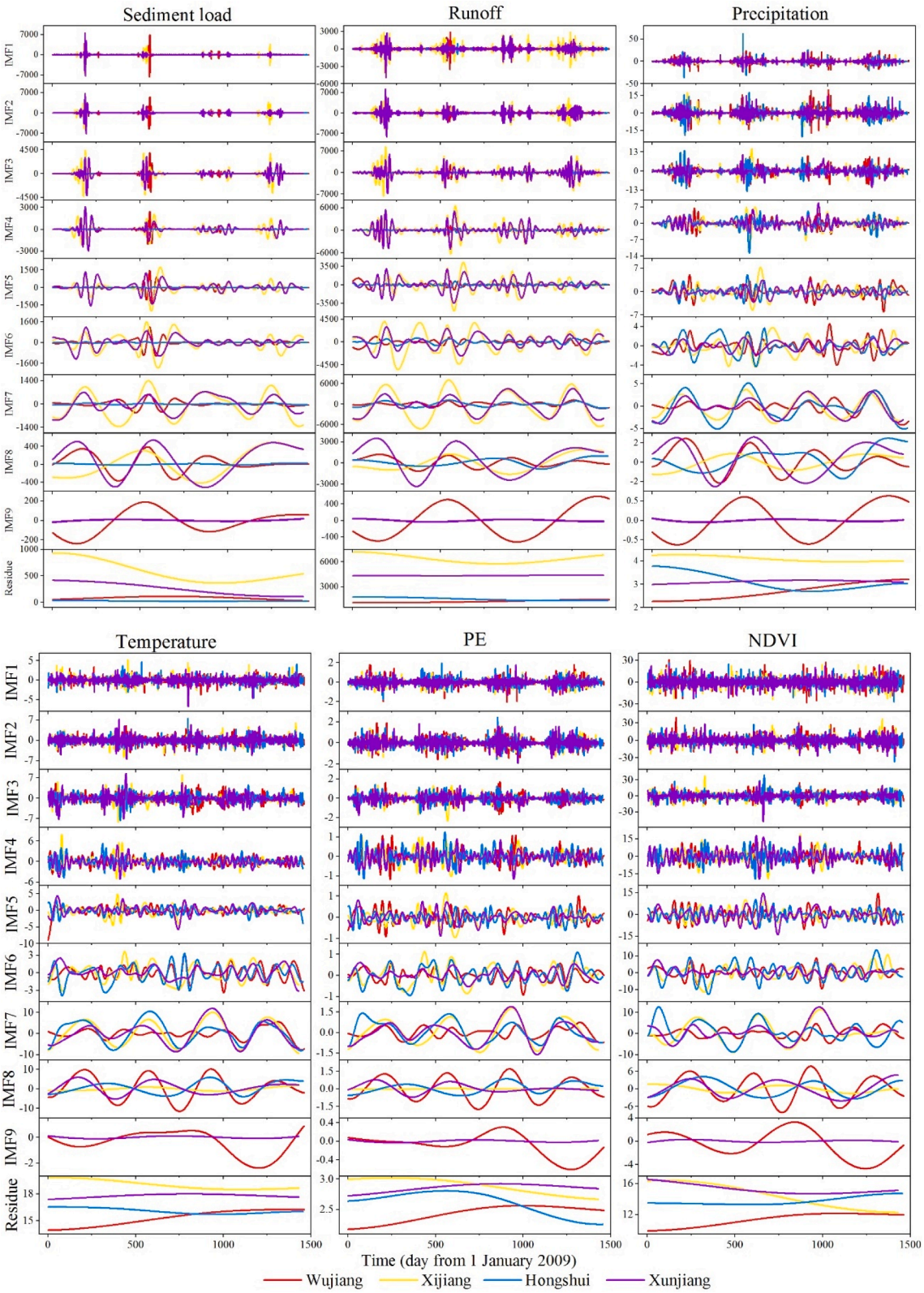

Fig. 4. Intrinsic mode function (IMF) and residue for daily suspended sediment load (SSL) and five potential variables (runoff, precipitation, temperature, potential evapotranspiration [PE], and normalized differential vegetation index [NDVI]) affecting daily SSL at Wujiang, Xijiang, Hongshui, and Xujiang karst catchments.

Borrelli et al., 2020). Interestingly, compared with the CV values for monthly and annual SSL (Shi et al., 2013; Li et al., 2016; Li et al., 2017b; Li et al., 2020b), those for daily SSL were much higher, indicating that capturing reliable data on daily SSL dynamics is difficult.

Fig. 2 shows the temporal variation in daily SSL and the five variables of runoff, precipitation, air temperature, PE, and NDVI. Throughout the study period, daily SSL values were relatively low, with large values observed intermittently, implying high variability, especially in Wujiang catchment. Runoff, precipitation, and NDVI values exhibited seasonal variations, with high values in summer and low

Table 3
Scale of each intrinsic mode function (IMF) of daily suspended sediment load (SSL) and five potential variables affecting daily SSL in the four karst catchments.

		Sediment load	Runoff	Precipitation	Temperature	PE	NDVI	Mean
Wujiang	IMF1	4	3	4	4	4	4	4
	IMF2	5	6	6	6	6	6	6
	IMF3	8	13	11	12	11	11	11
	IMF4	22	23	20	23	22	19	21
	IMF5	36	28	24	22	40	35	31
	IMF6	25	41	47	52	46	39	42
	IMF7	211	70	33	42	36	104	83
	IMF8	483	33	365	196	266	173	253
	IMF9	758	761	758	50	8	750	514
Xijiang	IMF1	4	4	4	4	4	4	4
	IMF2	7	8	8	8	7	7	7
	IMF3	12	16	13	13	15	13	14
	IMF4	19	29	27	28	29	26	26
	IMF5	34	48	45	40	58	40	44
	IMF6	87	87	44	39	48	32	56
	IMF7	125	159	260	318	358	18	206
	IMF8	745	744	747	750	35	742	627
Hongshui	IMF1	4	3	4	4	4	3	3
	IMF2	6	6	6	6	6	6	6
	IMF3	7	12	10	11	12	12	11
	IMF4	13	25	21	19	22	21	20
	IMF5	36	38	41	42	38	34	38
	IMF6	71	49	52	42	38	28	47
	IMF7	291	171	55	364	263	50	199
	IMF8	224	73	117	501	499	507	320
Xunjiang	IMF1	4	4	4	4	4	4	4
	IMF2	7	8	7	7	7	7	7
	IMF3	8	15	13	15	14	13	13
	IMF4	16	31	25	22	23	24	23
	IMF5	66	63	61	47	41	38	52
	IMF6	87	119	136	72	45	33	82
	IMF7	106	260	73	220	169	23	142
	IMF8	56	41	33	502	20	496	191
	IMF9	762	752	264	415	323	263	463

PE: potential evapotranspiration; NDVI: normalized differential vegetation index.

values in winter. For one year, air temperature and PE showed an unvarying pattern like a downward parabola. The M−K test indicated that daily precipitation in the four catchments showed a significantly increasing trend ($P < 0.01$; Table 2). Significant increasing trends in daily runoff were observed in three of the four catchments ($P < 0.01$), except Hongshui catchment, which had a significantly decreasing trend ($P < 0.01$). In Wujiang and Xijiang catchments, daily SSL exhibited a significantly decreasing trend, whereas a significantly increasing trend was found in Hongshui and Xunjiang catchments ($P < 0.01$; Table 2).

As expected, daily SSL was positively and significantly correlated with runoff, precipitation, and air temperature ($P < 0.01$; Fig. 3). This result is in accordance with the findings of a number of previous studies (Wu et al., 2012; Li et al., 2016; Vercruysse et al., 2017; Wang et al., 2017a; Zhao et al., 2017). Although no significant relationship was observed between daily SSL and PE in Wujiang catchment ($P = 0.20$), daily SSL was significantly correlated with PE in the other three catchments, with coefficients of determination ranging from 0.01 to 0.03 ($P < 0.01$; Fig. 3). There were no statistically significant relationships between daily SSL and NDVI values in Wujiang ($P = 0.33$) and Xijiang ($P = 0.33$) catchments, whereas the NDVI was negatively correlated with daily SSL in Hongshui and Xunjiang catchments ($P < 0.05$; Fig. 3). Previous studies indicated that a high NDVI usually corresponds to low sediment load at the annual scale (Zhou et al., 2008; García-Ruiz, 2010; Zhang et al., 2016), whereas a positive relationship was observed between the NDVI and sediment load at the monthly scale (Ouyang et al., 2010; Li et al., 2017b; Huang et al., 2019). Therefore, the relationship between sediment load and the NDVI is complex and dependent on the temporal scale (Duan et al., 2016; Borrelli et al., 2017; Starke et al., 2020).

4.2. Memd

Using the MEMD method, each multivariate dataset was decomposed into eight (Xijiang and Honghsui catchments) or nine IMFs (Wujiang and Xunjiang catchments) and one residue (Fig. 4). The number of IMFs in the present study was considerably higher than that in previous studies, which decomposed the dataset into three or four IMFs (She et al., 2014; Liu et al., 2018b; Zhao et al., 2018; Liu et al., 2019; Yang et al., 2019b; Yang et al., 2022). Differences in the number of samples account for the variation. The previous studies included 21–45 samples, whereas the present one included 1,400 samples. Thus, more IMFs were required to capture information on the variables at multiple scales in the present study. With an increase in the IMF number, the frequency oscillation decreased, and hence the corresponding representative temporal scale increased. As a result, IMFs with lower numerical values generally had greater frequency oscillations, whereas lower frequency oscillations were generated at large scales (Rehman and Mandic, 2010; Hu et al., 2014).

For each multivariate dataset, the oscillation scales of the same IMF were very similar among the variables, and accurate scales were computed from instantaneous frequencies through Hilbert transform analysis (Table 3). The mean timescales of the four IMFs (IMF1, IMF2, IMF3, and IMF4) for the four catchments were very close, indicating that the four karst catchments exhibited similar SSL dynamics and its associated factors at relatively short time intervals of about 4, 7, 12, and 23 days, respectively. At longer timescales from IMF 5 to IMF 9, the mean IMFs for the four catchments varied considerably. For example, the mean IMF5 was 83 days in Wujiang catchment, whereas it was 206 days in Xijiang catchment (Table 3). This result implies that the underlying processes controlling daily SSL differ significantly in karst catchments at longer time intervals. Furthermore, as the mode index increased, the differences in the IMF scales among different variables became larger in

Table 4
Percentage of variance explained by each intrinsic mode function (IMF) or residue in the four karst catchments.

		Sediment load	Runoff	Precipitation	Temperature	PE	NDVI
Wujiang	IMF1	40.1	7.12	49.0	0.76	5.74	20.6
	IMF2	35.6	6.33	31.0	2.08	7.71	25.6
	IMF3	24.7	8.60	17.9	3.42	7.97	19.8
	IMF4	14.6	4.39	6.96	2.53	5.55	11.4
	IMF5	11.0	10.6	7.66	2.26	4.32	7.80
	IMF6	11.9	18.1	5.71	2.23	4.11	5.39
	IMF7	7.07	26.1	6.99	10.2	7.34	2.66
	IMF8	7.74	38.1	4.57	62.5	48.6	11.9
	IMF9	3.07	13.7	0.68	1.35	3.27	3.48
	Residue	0.14	1.65	0.36	1.13	0.92	0.41
	Total	156	135	131	88.5	95.6	109
Xijiang	IMF1	11.5	1.52	39.6	1.38	6.33	21.6
	IMF2	19.4	4.05	29.7	3.95	11.0	34.1
	IMF3	28.4	10.4	23.1	5.71	13.8	31.0
	IMF4	13.1	8.76	12.7	4.31	8.46	16.5
	IMF5	9.16	6.62	8.98	4.27	7.20	8.49
	IMF6	17.4	17.7	8.82	5.13	13.1	11.4
	IMF7	27.8	65.5	17.4	71.0	59.5	19.3
	IMF8	4.00	4.65	1.66	1.61	0.06	0.76
	Residue	1.72	0.83	0.05	0.58	1.10	1.68
	Total	133	120	142	98.0	121	145
Hongshui	IMF1	14.9	2.94	43.5	1.18	6.99	18.6
	IMF2	18.8	3.86	29.6	3.29	9.16	26.8
	IMF3	29.5	6.28	20.9	4.74	11.2	31.6
	IMF4	10.8	4.03	10.9	3.87	8.05	17.0
	IMF5	8.52	3.63	3.95	2.54	3.90	7.46
	IMF6	22.3	13.7	7.65	4.90	12.9	17.7
	IMF7	35.7	45.8	22.8	64.3	38.6	16.5
	IMF8	8.19	29.3	3.97	21.8	13.0	4.34
	Residue	0.88	3.26	0.40	0.22	2.43	0.18
	Total	150	113	144	107	106	140
Xunjiang	IMF1	17.4	1.37	37.8	1.28	6.22	19.7
	IMF2	28.0	7.34	25.6	4.10	12.6	35.0
	IMF3	28.1	10.7	19.5	6.82	11.1	28.0
	IMF4	20.0	12.4	10.7	3.73	7.35	21.4
	IMF5	13.4	8.44	4.68	4.26	5.17	14.1
	IMF6	13.8	11.5	3.06	2.32	4.66	3.78
	IMF7	17.2	48.0	14.7	62.9	46.2	11.8
	IMF8	9.42	26.5	8.76	20.7	9.23	4.79
	IMF9	0.00	0.00	0.00	0.01	0.03	0.02
	Residue	0.90	0.01	0.01	0.07	0.24	0.24
	Total	148	126	125	106	103	139

PE: potential evapotranspiration; NDVI: normalized differential vegetation index.

a given catchment (Table 3). Therefore, the MEMD method was sufficient to isolate the common scales for daily SSL for the numbers of low IMFs, while the common scales did not appear at longer time intervals for all variables. This was likely due to the Heisenberg uncertainty principle and limited number of cycles included in the IMFs at long timescales (Hu and Si, 2013; Hu et al., 2014; Zhao et al., 2018; Yang et al., 2019a).

Variance in the percentage of daily SSL produced by different IMFs and their residues in the four catchments are presented in Table 4. Short timescale oscillations (e.g., IMF1 to IMF4) contributed 72–115 % of the total variance in daily SSL, indicating that the dominant processes influencing temporal variations in SSL at short time intervals of about 4–23 days (Tables 3 and 4). This result could improve the understanding of suspended sediment load dynamics of the karst watersheds and might optimize sampling strategies for daily suspended sediment load measurements. Similarly, short timescales exerted a substantial influence on precipitation and PE in the original time series. In contrast, long timescales governed runoff, air temperature, and NDVI variations (Table 4). The variance contributions of the residue to all the variables in the four catchments accounted for only 0–3.3 % of the total variance, which was much lower than that found in previous studies (She et al., 2017; Zhao et al., 2018; Zhu et al., 2021; Yang et al., 2022). The high number of observations and samples in the current study explain this finding. Interestingly, the sum of the variance did not reach 100 % for any of the variables. The latter may be explained by related temporal processes not being independent at different timescales or the scale components generated by MEMD not being perfectly orthogonal (Champa et al., 2010; Wang et al., 2017b). With this advantage, the MEMD is well suited to nonstationary and nonlinear data series (Rehman and Mandic, 2010; Hu et al., 2014).

4.3. Scale-dependent relationships between daily SSL and associated variables

Pearson's correlation coefficients for daily SSL and the five potential variables (runoff, precipitation, air temperature, PE, and NDVI) affecting daily SSL for each IMF and residue are shown in Fig. 5. As shown by the results, the residue term for daily SSL was significantly correlated with all the variables in the four catchments ($P < 0.01$), except the NDVI in Wujiang watershed (P greater than 0.05). This finding is in accordance with that reported in previous studies (Hu and Si, 2013; She et al., 2017; Liu et al., 2019; Zhu et al., 2021; Yang et al., 2022). Unlike the residue, the relationships between daily SSL and associated variables differed considerably for different IMFs (Fig. 5). In most cases, the correlation coefficients between daily SSL and air temperature, PE, and NDVI values were all significant at long timescales of IMF5 to IMF9 ($P < 0.01$), indicating that these three variables were large-scale dependence factors influencing daily SSL. Both daily SSL and runoff were significantly correlated with all IMFs in the four karst catchments ($P < 0.01$), implying that runoff is a critical variable

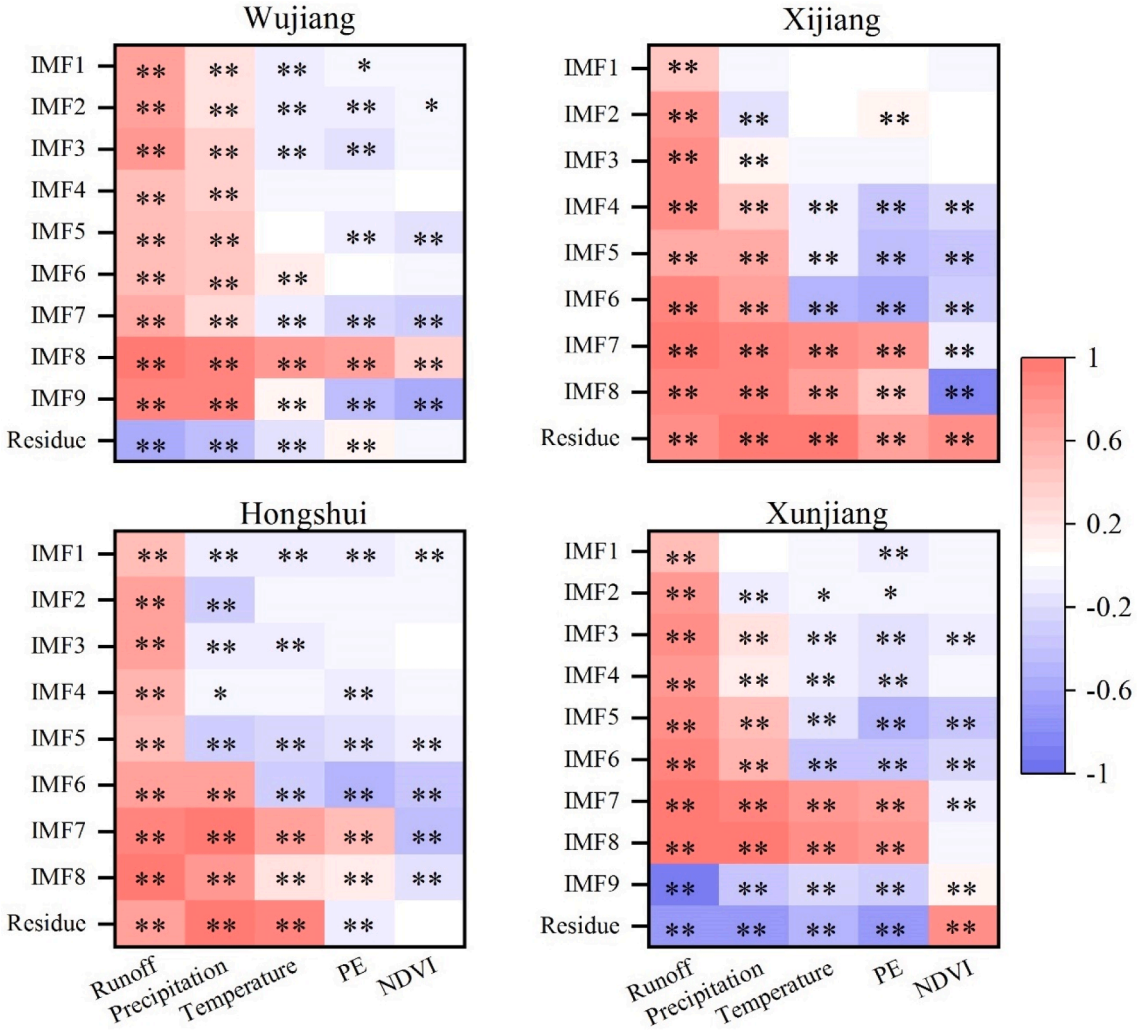

Fig. 5. Pearson's correlation coefficients for daily suspended sediment load (SSL) and five potential variables (runoff, precipitation, temperature, potential evapotranspiration [PE], and normalized differential vegetation index [NDVI]) affecting daily SSL at Wujiang, Xijiang, Hongshui, and Xujiang karst catchments. * Indicates $P < 0.05$; ** Indicates $P <$ 0 0.01.

influencing daily SSL at all timescales. Similar to runoff, a significant relationship was found between daily SSL and precipitation at all IMFs, except IMF1 in Xijiang catchment (Fig. 5).

It is worth noting that each variable was significantly correlated with daily SSL at several IMFs, although no significant correlation was detected at the observation scale. Although no significant relationship was observed between daily SSL and the NDVI in Wujiang and Xijing catchments at the observation scale (Fig. 3), this relationship was significant at IMF2, IMF5, IMF7 − 9 in Wujiang catchment and IMF4 − 8 in Xijiang catchment. The lack of a significant correlation at the observation scale was defined arbitrarily as a goal and does not denote the lack of significant relationships between the daily sediment load and associated variables. This further corroborates the idea that measurements at a single scale (i.e., daily scale) are not sufficient to capture information about scale-dependent relationships between daily SSL and SSL-related variables (Hu and Si, 2013; Zhao et al., 2018). As reported previously, correlations between daily sediment load and specific variables can change from significantly negative to significantly positive at different IMFs (Sang et al., 2014; Meng et al., 2019; Zhao et al., 2021). In this way, positive or negative effects at one scale can be cancelled by the opposite effects at other scales, resulting in low overall correlations for the original data at the observation scale (She et al., 2014; Taesam and Ouarda, 2019; Wen et al., 2019).

4.4. *Multiscale prediction functions of daily SSL*

Daily SSL at each IMF or residue were estimated from scale-specific associated variables at the corresponding IMF or residue using multiple stepwise linear regression (Table 5). The number of predictors increased with the timescale. The relative importance of each predictor was evaluated by standardized regression coefficients (Table 5). The predictor and its corresponding relative importance to daily SSL differed with the timescale. However, runoff appeared in each equation for all four karst catchments, implying that runoff exerts a strong influence on daily SSL at both short and long timescales. The value of coefficient of variation (R^2) between daily SSL and scale-specific factors exhibited an increasing trend in accordance with the timescale (Table 5). Hence, sediment transport processes were most likely deterministic at longer timescales.

By adding all the estimated IMFs and residues, daily SSL at the observational scale was predicted for each karst catchment (Fig. 6). The model performance of the daily SSL before and after MEMD was compared. The R^2 obtained from MEMD were significantly greater than the corresponding values obtained from the undecomposed data series ($P < 0.01$; Fig. 6). Similarly, the *AIC* and *RMSE* values calculated from the observed and predicted scale-dependent values of daily SSL at the observation scale were much lower than those of the original data, which did not consider scale dependency. By separating daily SSL and

Table 5
Stepwise multiple linear regression (MLR) between daily suspended sediment load (SSL) and five potential variables affecting daily SSL at each intrinsic mode function (IMF) or residue using multivariate empirical mode decomposition (MEMD) in the four karst catchments.

	IMF	Model	R^2	F
Wujiang	IMF1	7.51 + 1.04(0.67) RF + 19.6(0.18) P + 3.22(0.04) NDVI	0.49	470
	IMF2	−3.02 + 1.10(0.71) RF + 31.6(0.24) P + 21.7(0.06) T	0.56	620
	IMF3	7.45 + 0.80(0.72) RF + 29.1(0.20) P + 14.8(0.25) NDVI-175(0.20) PE + 28.0 (0.12) T	0.64	510
	IMF4	0.56 + 0.53(0.44) RF + 72.0(0.40) P + 222(0.27) PE-20.3(0.10) T	0.36	208
	IMF5	−14.7 + 0.24(0.36) RF + 59.4(0.40) P + 172.4(0.22) PE	0.34	247
	IMF6	13.6 + 0.22(0.42) RF + 40.8(0.23) P + 38.1(0.19) T + 13.5(0.17) NDVI-125 (0.15) PE	0.33	141
	IMF7	4.19 + 0.46(1.34) RF-98.4(0.79) P-71.7 (0.15) PE + 6.69(0.08) NDVI	0.66	706
	IMF8	−2.84 + 0.02(0.08) RF-44.4(1.02) NDVI + 76.7(0.48) P + 83.0(0.42) PE + 23.0(0.75) T	0.96	7.3×10^3
	IMF9	1.18 + 414(1.59) P + 1105(2.28) PE-233(1.77) T + 35.1(0.69) NDVI + 0.42 (1.37) RF	1.00	1.5×10^5
	Residue	−954 + 1.09(5.64) RF + 620(3.16) PE −676(8.70) P	1.00	3.9×10^5
Xijiang	IMF1	12.9 + 0.36(0.04) RF	0.20	34
	IMF2	0.65 + 0.50(0.78) RF + 32.7(0.06) T-5.02(0.05) NDVI	0.60	698
	IMF3	5.42 + 0.41(0.84) RF + 25.4(0.05) T	0.70	1.6×10^3
	IMF4	−10.8 + 0.32(0.89) RF + 30.5(0.08) T-12.1(0.11) NDVI-30.5(0.11) P	0.71	889
	IMF5	−4.32 + 0.17(0.48) RF + 85.8(0.31) P-831(0.57) PE + 61.6(0.46) NDVI + 26.2 (0.02) T	0.59	408
	IMF6	−21.5 + 0.23(0.78) RF-77.5(0.18) T-138(0.09) PE + 7.48(0.05) NDVI	0.82	1.6×10^3
	IMF7	8.08 + 0.19(0.98) RF-531(0.60) PE + 55.1(0.38) T + 18.6(0.12) NDVI + 68.8 (0.20) P	0.98	1.2×10^4
	IMF8	−0.66 + 494(1.15) P + 0.24(0.87) RF-173(0.48) T + 172(0.59) NDVI-605 (0.06) PE	1.00	1.4×10^6
	Residue	−3980 + 26.6(0.07) T + 0.29(0.70) RF + 758(0.47) PE	1.00	6.4×10^7
Hongshui	IMF1	−0.26 + 0.06(0.48) RF-1.89(0.07) T-0.26(0.05) P	0.25	160
	IMF2	0.43 + 0.07(0.63) RF-0.80(0.12) P-0.18 (0.05) NDVI	0.46	414
	IMF3	−0.50 + 0.08(0.71) RF-1.67(0.17) P	0.51	748
	IMF4	−0.96 + 0.05(0.57) RF-1.44(0.17) P-0.33(0.10) NDVI + 1.99(0.16) T-6.44 (0.14) PE	0.34	149
	IMF5	0.22 + 0.0.44(0.57) RF −6.76(0.54) P-7.82(0.13) PE-1.35(0.10) T	0.49	343
	IMF6	−0.02 + 0.03(0.44) RF + 5.36(0.37) P	0.55	884
	IMF7	0.29 + 16.6(1.56) *P*-1.89(0.34) T + 0.86 (0.14) NDVI-5.03(0.13) PE-0.10(0.20) RF	0.91	3.1×10^3
	IMF8	0.79 + 0.03(1.15) RF-2.96(0.52) NDVI-5.13(0.43) P + 3.95(0.85) T-16.3(0.51) PE	0.97	8.6×10^3
	Residue	22.15 + 4.43(0.35) P-18.9(0.77) PE + 0.02(0.90) RF	1.00	1.1×10^{11}
Xunjiang	IMF1	4.23 + 0.50(0.47) RF-111(0.07) PE	0.22	205
	IMF2	4.90 + 0.48(0.81) RF + 15.1(0.07) P + 36.0 (0.08) T-123(0.08) PE	0.63	604
	IMF3	−2.65 + 0.41(0.84) RF + 37.9(0.15) P + 28.0(0.08) T-143(0.09) PE	0.74	1.0×10^3
	IMF4	−8.74 + 0.30(0.80) RF-21.8 (0.05) T	0.64	1.3×10^3
	IMF5	9.97 + 0.29(0.28) T-551(0.34) PE-26.5 (0.07) P	0.73	958
	IMF6	−12.3 + 0.36(1.10) RF-82.2(0.18) P + 281(0.16) PE-20.6(0.11) NDVI	0.86	2.2×10^3
	IMF7	2.78 + 0.32(1.80) RF-206(0.89) *P*-3.57 (0.03) NDVI	0.91	4.6×10^3
	IMF8	−12.3 + 573(2.58) P + 235(0.23) PE + 82.5(0.59) NDVI-0.20(1.12) RF-95.4 (0.79) T	1.00	5.5×10^3
	IMF9	−0.12–1.19(3.70) RF + 348 (7.25) NDVI + 2205(7.90) P-5.79(0.06) T	1.00	1.1×10^6
	Residue	−11886 + 303(1.57) NDVI + 546(0.85) T-0.51(0.13) RF	1.00	7.5×10^7

Number in parenthesis is the standardized regression coefficient; F: statistics for the accepted models; RF: runoff; P: precipitation; T: temperature; PE: potential evapotranspiration; NDVI: normalized differential vegetation index.

SSL-associated variables into different timescales, MEMD provides additional information on the factors influencing sediment transport (Liu et al., 2018a; Yang et al., 2022). As a result, MEMD rather than the original undecomposed data series sheds light on scale-dependent temporal relationships of daily SSL and environmental factors in nonlinear and nonstationary systems (Liu et al., 2018b; Zhu et al., 2021). Therefore, the MEMD method can enhance daily SSL predictions.

In present study, we also quantified the scale-dependent relationships between daily suspended sediment load and precipitation and NDVI, and to predict daily SSL based on these relationships. The daily SSL at each IMF or residue estimated from scale-specific associated variables using MLR was presented in Table S1. However, the daily SSL at each IMF or residue were poorly estimated using only with precipitation and NDVI. For the R^2, 60 % and 72 % of the values were lower than 0.5 and 0.8, respectively (Table S1). By adding all the estimated IMFs and residues, daily SSL at the observational scale was predicted for each karst catchment (Fig. S1). The *AIC* and *RMSE* using only precipitation and NDVI were much greater than the corresponding *AIC* and *RMSE* values using all the five potential influencing variables. As expected, the R^2 values using only precipitation and NDVI were ranging from 0.098 to 0.200, which were much lower than those using all the five potential influencing variables. Therefore, the five potential influencing factors of runoff, precipitation, temperature, potential evapotranspiration, and NDVI were selected in current study.

To quantify the relative importance of each scale in the predictive model, the R^2 between overall daily SSL at the observation scale and each predicted IMF or residue was calculated, as shown in Fig. 7. The R^2 differed considerably between different IMFs and karst catchments. IMF2, IMF3, IMF5, and IMF7 were the principal contributors to the overall predictions of daily SSL (Fig. 7). Specifically, IMF2, IMF3, and IMF4 explained major variation in daily SSL predictions in Wujiang and Xunjiang catchments, whereas the IMF2, IMF3, and IMF7 were the primary contributors to overall predictions of daily SSL in Xijiang and Hongshui catchments. As the representative of longer timescales, residue explained a relatively low amount of variation in daily SSL predictions in all four catchments. This result differs from that of some previous studies, which found that residue accounted for a relatively large amount of variation in soil hydraulic properties or soil water content (Hu and Si, 2013; She et al., 2017; Zhao et al., 2018). Differences in the dominant processes operating at short and long timescales explain the discord.

Fig. 7b presents the R^2 between the total predicted daily SSL at different scales by each variable and the total predictions at the observation scale. Clearly, the relative importance of each explanatory variable in terms of daily SSL prediction at the observation scale was considerably different. Runoff was the dominant explanatory predictor of daily SSL in all four catchments (Fig. 7b). Due to their unique hydrogeological conditions, soil erosion and sediment transport

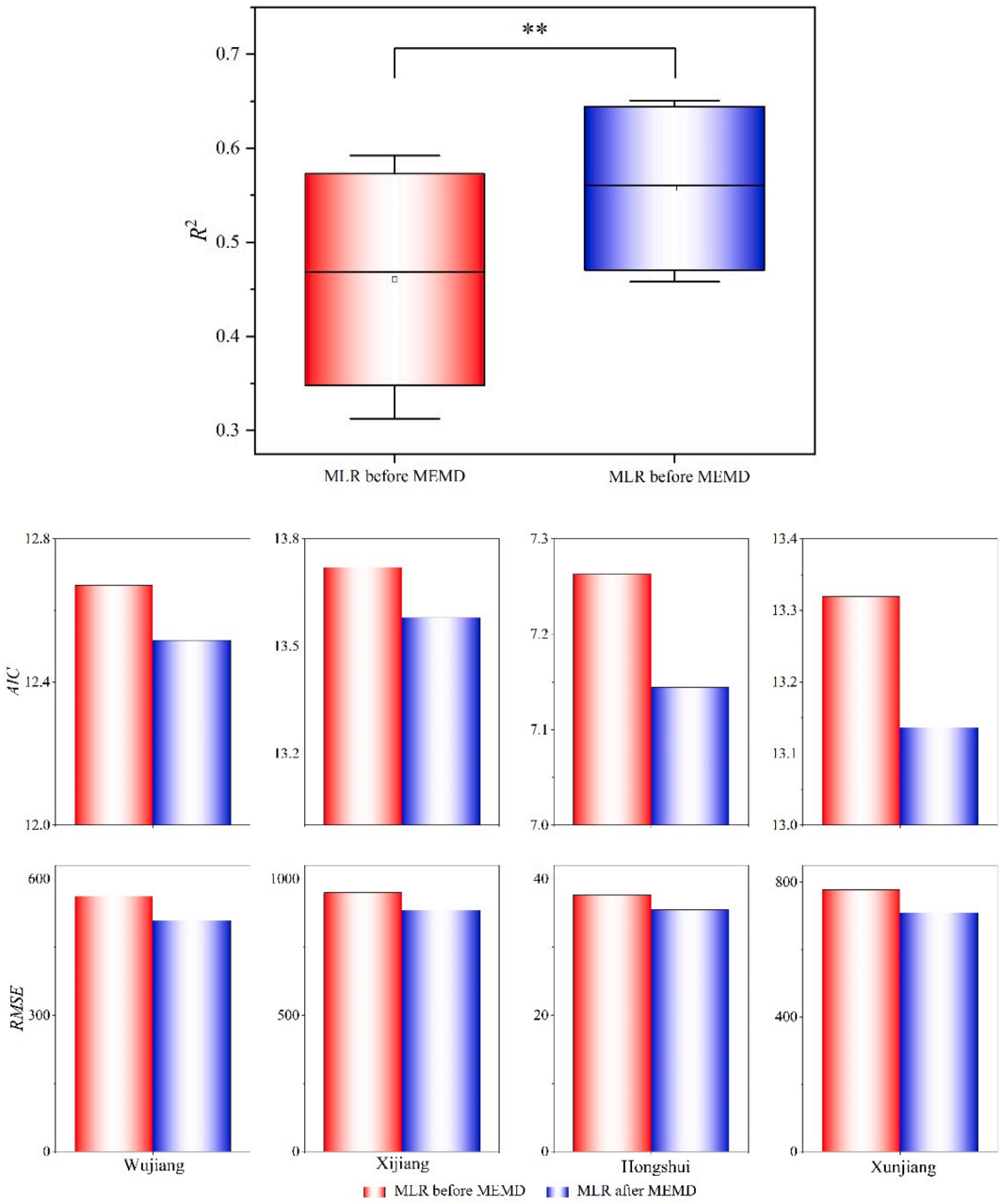

Fig. 6. Comparison of coefficient of determination (R^2), Akanke's Information Criterion (*AIC*), and root mean square error (*RMSE*) using a multiple linear regression (MLR) model before and after multiple empirical mode decomposition (MEMD). ** Indicates $P < 0.01$.

processes in karst regions are more complex than those in non-karst regions (Jiang et al., 2014; Wang et al., 2019; Li et al., 2020c). In karst regions, most precipitation seeps down into groundwater via fissures, fractures, and cracks, and therefore surface runoff generation differs widely, depending on the permeability of the epikarst and bedrock (Wilcox et al., 2008; Hartmann et al., 2014; Fischer et al., 2017). As a result, the surface runoff coefficient in karst regions is generally very low (Dai et al., 2017; Li et al., 2017c; Zhang et al., 2019). Peng and Wang (2012) indicated that large runoff and soil erosion were principally produced by rainstorms, with a maximum 30-min rainfall intensity over 30 mm h^{-1} and a rainfall depth greater than 40 mm in karst regions. When rainstorms follow a period of precipitation, they can generate large quantities of runoff and soil loss, as fissures, fractures, and cracks in the epikarst zone are fully saturated with rainwater (Hartmann et al., 2012; Jukić and Denić-Jukić, 2015; Cao et al., 2021). Therefore, soil erosion is probably more dependent on continuous rainfall or runoff in karst regions than in non-karst regions (Li et al., 2017a; Cao et al., 2020a). Moreover, eroded sediment from hillslopes frequently blocks conduits or sinkholes in karst depressions and results in waterlogging in these depressions after severe rainstorms of long durations (Li et al., 2019; Zhang *et al.*, 2020). Consequently, most runoff is eventually discharged into other karst catchments, and the eroded sediment is deposited in karst depressions (Jiang et al., 2014; Cao et al., 2020b). In this way, the unique hydrogeological conditions in karst regions may reduce or weaken the effects of rainfall and vegetation on soil erosion. Due to the sediment transport processes generally exhibit nonlinear and nonstationary characteristics, this study emphasizes the importance of the MEMD method in unravelling scale-dependent relationships between daily SSL and related variables in karst catchments.

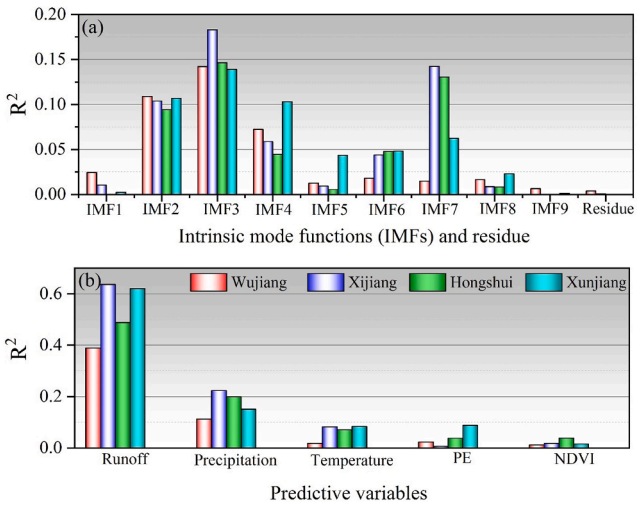

Fig. 7. Coefficient of determination (R^2) for daily suspended sediment load (SSL) at the observation scale and (a) its value predicted by each intrinsic mode function (IMF) or residue and (b) total daily SSL predicted by each of the five variables.

4.5. Limitations

The current study represents an initial undertaking aimed at identifying the scale- specific controls of daily suspended sediment load in karst catchments. Nevertheless, this study also has some limitations. Firstly, the period of observation for daily suspended sediment load is only 4 years which probably cannot reflect the long term hydrological and sediment transport processes. The relatively longer records of daily SSL is suggested to gain more accurate scale and deeper understanding of suspended sediment load transportation mechanisms in karst catchments. Furthermore, many cascade reservoirs have recently been constructed in this region (Wu et al., 2012; Li et al., 2020b). As a result, the operation and construction of large reservoirs or dams may identify as the significant cause of the drastic decline of sediment discharge (Jiang et al., 2014; Li et al., 2016; Wang et al., 2019). Therefore, quantitative analysis of the effect of reservoir construction on daily suspended sediment load is also required to have a more comprehensive understanding of the factor controlling daily SSL. Additionally, the 3D structure of the fracture or conduit networks is closely related to the hydrological or sediment connectivity of the karst catchments, and thus has a great influence on daily sediment load (Heckmann et al., 2018; Zhang et al., 2019). Hence, future studies are needed to quantify the influence of the karstic network structure and hydrological or sediment connectivity of the epikarst zone on sediment load in karst catchments.

5. Conclusions

We used the MEMD method to quantify scale-dependent relationships between daily SSL and runoff, precipitation, air temperature, PE, and NDVI values in four karst catchments in southwest China. Eight (Xijiang and Honghsui catchments) or nine (Wujiang and Xunjiang catchments) IMFs and a residue were obtained for daily SSL and five potential variables affecting SSL after MEMD. More than 72 % of the total variance in daily SSL was extracted from IMF1 to IMF4, implying that the dominant processes controlling the temporal variation in sediment load at short time intervals of approximately 4–23 days. With the aid of MEMD, daily SSL was significantly correlated with each of the five variables at least at one scale, with no statistically significant correlation found at the observation scale. Runoff showed the largest relative importance to the observation scale in the daily SSL prediction model. The prediction of daily SSL based on the IMFs and residue terms after MEMD were superior to the modelling results obtained using the original data. This study proved that MEMD can be used to identify scale-specific factors controlling daily SSL and hence the true scale of underlying processes influencing daily SSL. MEMD is an efficient method for obtaining valuable information about nonstationary and nonlinear data sequences, and it may be a superior choice for predicting daily SSL in catchments with different underlying surfaces.

Declaration of Competing Interest

The authors declare that they have no known competing financial interests or personal relationships that could have appeared to influence the work reported in this paper.

Data availability

Data will be made available on request.

Acknowledgements

This study was supported by the State Key Program of National Natural Science Foundation of China (41730748), National Natural Science Foundation of China (41977073), National Key Research and Development Program of China (2019YFE0116900), Guangxi Key Research and Development Program (AB20297004), Youth Innovation Promotion Association of CAS (2020359), and Science and Technology Innovation Program of Hunan Province (2021RC3115), and Natural Science Foundation of Hunan Province (2022JJ30646).

Appendix A. Supplementary data

Supplementary data to this article can be found online at https://doi.org/10.1016/j.catena.2022.106745.

References

Borrelli, P., Robinson, D.A., Fleischer, L.R., Lugato, E., Ballabio, C., Alewell, C., Meusburger, K., Modugno, S., Schütt, B., Ferro, V., 2017. An assessment of the global impact of 21st century land use change on soil erosion. Nature Communications 8, 1–13.

Borrelli, P., Robinson, D.A., Panagos, P., Lugato, E., Yang, J.E., Alewell, C., Wuepper, D., Montanarella, L., Ballabio, C., 2020. Land use and climate change impacts on global soil erosion by water (2015–2070). Proceedings of the National Academy of Sciences 117, 1–8.

Cao, L., Wang, S., Peng, T., Cheng, Q., Fryer, A.E., 2020a. Monitoring of suspended sediment load and transport in an agroforestry watershed on a karst plateau. Southwest China. Agriculture Ecosystems & Environment 299, 106976.

Cao, L., Liu, S., Wang, S., Cheng, Q., Fryar, A.E., Zhang, L., Zhang, Z., Yue, F., Peng, T., 2021. Factors controlling discharge-suspended sediment hysteresis in karst basins, Southwest China: Implications for sediment management. Journal of Hydrology 594, 125792.

Cao, Z., Zhang, Z., Zhang, K., Wei, X., Yang, Z., 2020b. Identifying and estimating soil erosion and sedimentation in small karst watersheds using a composite fingerprint technique. Agriculture, Ecosystems & Environment 294, 106881.

Champa, Joshi, Binayak, P., Mohanty, 2010. Physical controls of near-surface soil moisture across varying spatial scales in an agricultural landscape during SMEX02. Water Resources Research 46, 65-74.

Cook, T.L., Yellen, B.C., Woodruff, J.D., Miller, D., 2015. Contrasting human versus climatic impacts on erosion. Geophysical Research Letters 42, 6680–6687.

Dai, Q., Peng, X., Yang, Z., Zhao, L., 2017. Runoff and erosion processes on bare slopes in the Karst Rocky Desertification Area. Catena 152, 218–226.

de Vente, J., Poesen, J., Verstraeten, G., Govers, G., Vanmaercke, M., Van Rompaey, A., Arabkhedri, M., Boix-Fayos, C., 2013. Predicting soil erosion and sediment yield at regional scales: where do we stand? Earth-Science Reviews 127, 16–29.

Duan, L., Huang, M., Zhang, L., 2016. Differences in hydrological responses for different vegetation types on a steep slope on the Loess Plateau, China. Journal of Hydrology 537, 356–366.

Fischer, P., Jardani, A., Wang, X., Jourde, H., Lecoq, N., 2017. Identifying flow networks in a karstified aquifer by application of the Cellular Automata-Based Deterministic Inversion Method (Lez Aquifer, France). Water Resources Research 53, 10508–10522.

Gao, G., Ma, Y., Fu, B., 2016. Multi-temporal scale changes of streamflow and sediment load in a loess hilly watershed of China. Hydrological Processes 30, 365–382.

García-Ruiz, J.M., 2010. The effects of land uses on soil erosion in Spain: A review. Catena 81, 1–11.

Hartmann, A., Lange, J., Aguado, À.V., Mizyed, N., Smiatek, G., Kunstmann, H., 2012. A multi-model approach for improved simulations of future water availability at a large Eastern Mediterranean karst spring. Journal of Hydrology 468, 130–138.
Hartmann, A., Goldscheider, N., Wagener, T., Lange, J., Weiler, M., 2014. Karst water resources in a changing world: Review of hydrological modeling approaches. Reviews of Geophysics 52, 218–242.
Heckmann, T., Cavalli, M., Cerdan, O., Foerster, S., Javaux, M., Lode, E., Smetanóva, A., Vericat, D., Brardinoni, F., 2018. Indices of sediment connectivity: opportunities, challenges and limitations. Earth-Science Reviews 187, 77–108.
Hu, W., Biswas, A., Si, B.C., 2014. Application of multivariate empirical mode decomposition for revealing scale-and season-specific time stability of soil water storage. Catena 113, 377–385.
Hu, W., Si, B.C., 2013. Soil water prediction based on its scale-specific control using multivariate empirical mode decomposition. Geoderma 193, 180–188.
Huang, N.E., Shen, Z., Long, S.R., Wu, M.C., Shih, H.H., Zheng, Q., Yen, N.C., Tung, C.C., Liu, H.H., 1998. The empirical mode decomposition and the Hilbert spectrum for nonlinear and non-stationary time series analysis. Proceedings of the Royal Society of London. Series A: Mathematical, Physical and Engineering Sciences 454, 903-995.
Huang, X., Fang, N.F., Shi, Z.H., Zhu, T.X., Wang, L., 2019. Decoupling the effects of vegetation dynamics and climate variability on watershed hydrological characteristics on a monthly scale from subtropical China. Agriculture Ecosystems & Environment 279, 14–24.
Jiang, Z., Lian, Y., Qin, X., 2014. Rocky desertification in Southwest China: Impacts, causes, and restoration. Earth-Science Reviews 132, 1–12.
Jukić, D., Denić-Jukić, V., 2015. Investigating relationships between rainfall and karst-spring discharge by higher-order partial correlation functions. Journal of hydrology 530, 24–36.
Kendall Maurice, G., 1975. Rank correlation methods. Charles Griffin & Company Ltd, London, England.
Knapen, A., Poesen, J., Govers, G., Gyssels, G., Nachtergaele, J., 2007. Resistance of soils to concentrated flow erosion: A review. Earth Science Reviews 80, 75–109.
Li, Z., Xu, X., Zhu, J., Xu, C., Wang, K., 2020c. The contributions of the largest erosive events to sediment yields in karst catchments. Water Resources Research 56, e2019WR025839.
Li, D., Lu, X., Overeem, I., Walling, D.E., Syvitski, J., Kettner, A.J., Bookhagen, B., Zhou, Y.J., Zhang, T., 2021. Exceptional increases in fluvial sediment fluxes in a warmer and wetter High Mountain Asia. Science 374, 599–603.
Li, L., Ni, J., Chang, F., Yue, Y., Frolova, N., Magritsky, D., Borthwick, A.G.L., Ciais, P., Wang, Y., Zheng, C., 2020a. Global trends in water and sediment fluxes of the world's large rivers. Science Bulletin 65, 62–69.
Li, R., Xiong, L., Xiong, B., Li, Y., Xu, C.Y., 2020b. Investigating the downstream sediment load change by an index coupling effective rainfall information with reservoir sediment trapping capacity. Journal of Hydrology 125200.
Li, Z., Xu, X., Yu, B., Xu, C., Liu, M., Wang, K., 2016. Quantifying the impacts of climate and human activities on water and sediment discharge in a karst region of southwest China. Journal of Hydrology 542, 836–849.
Li, Z., Xu, X., Liu, M., Li, X., Zhang, R., Wang, K., Xu, C., 2017a. State-space prediction of spring discharge in a karst catchment in southwest China. Journal of Hydrology 549, 264–276.
Li, Z., Xu, X., Xu, C., Liu, M., Wang, K., Yi, R., 2017b. Monthly sediment discharge changes and estimates in a typical karst catchment of southwest China. Journal of Hydrology 555, 95–107.
Li, Z., Xu, X., Xu, C., Liu, M., Wang, K., Yu, B., 2017c. Annual runoff is highly linked to precipitation extremes in karst catchments of southwest China. Journal of Hydrometeorology 18, 2745–2759.
Li, Z., Xu, X., Zhang, Y., Wang, K., Zeng, P., 2019. Reconstructing recent changes in sediment yields from a typical karst watershed in southwest China. Agriculture, Ecosystems & Environment 269, 62–70.
Liu, Y., Song, H., An, Z., Sun, C., Zeng, X., 2020. Recent anthropogenic curtailing of Yellow River runoff and sediment load is unprecedented over the past 500 y. Proceedings of the National Academy of Sciences 117, 201922349.
Liu, Z., Ma, D., Hu, W., Li, X., 2018b. Land use dependent variation of soil water infiltration characteristics and their scale-specific controls. Soil and Tillage Research 178, 139–149.
Liu, Z., Matan, R., Rony, W., 2019. Spatial variation of soil water repellency in a commercial orchard irrigated with treated wastewater. Geoderma 333, 214–224.
Liu, H., Zhang, M., Lin, Z., Xu, X., 2018a. Spatial heterogeneity of the relationship between vegetation dynamics and climate change and their driving forces at multiple time scales in Southwest China. Agricultural & Forest Meteorology 256, 10–21.
Looney, D., Hemakom, A., Mandic, D., 2015. Intrinsic multi-scale analysis: a multi-variate empirical mode decomposition framework. Proc Math Phys Eng Sci 471, 20140709.
Ma, Y., Huang, H.Q., Xu, J., Brierley, G.J., Yao, Z., 2010. Variability of effective discharge for suspended sediment transport in a large semi-arid river basin. Journal of Hydrology 388, 357–369.
Mann, H.B., 1945. Nonparametric tests against trend. Econometrica: Journal of the Econometric Society 245–259.
Mccoll, K.A., 2020. Practical and theoretical benefits of an alternative to the Penman–Monteith evapotranspiration equation. Water Resources Research 56, e2020WR027106.
Meng, E., Huang, S., Huang, Q., Fang, W., Wu, L., Wang, L., 2019. A robust method for non-stationary streamflow prediction based on improved EMD-SVM model. Journal of Hydrology 568, 462–478.
Ouyang, W., Hao, F., Skidmore, A.K., Toxopeus, A., 2010. Soil erosion and sediment yield and their relationships with vegetation cover in upper stream of the Yellow River. Science of the Total Environment 409, 396–403.
Peng, T., Wang, S., 2012. Effects of land use, land cover and rainfall regimes on the surface runoff and soil loss on karst slopes in southwest China. Catena 90, 53–62.
Rehman, N., Mandic, D.P., 2009. Empirical Mode Decomposition. Multivariate EMD, Multivariate Synchrosqueezing, Matlab Code and Data http://www.commsp.ee.ic.ac.uk/mandic/research/emd.htm.
Rehman, N., Mandic, D.P., 2010. Multivariate empirical mode decomposition. Proceedings Mathematical Physical & Engineering Sciences 466, 1291–1302.
Rice, J.S., Emanuel, R.E., Vose, J.M., 2016. The influence of watershed characteristics on spatial patterns of trends in annual scale streamflow variability in the continental U. S. Journal of Hydrology 540, 850–860.
Rilling, G., 2007. http://perso.ens-lyon.fr/patrick.flandrin/emd.html.
Sang, Y.F., Wang, Z., Liu, C., 2014. Comparison of the MK test and EMD method for trend identification in hydrological time series. Journal of Hydrology 510, 293–298.
She, D., Tang, S., Shao, M.a., Xia, Y., 2014. Characterizing scale specific depth persistence of soil water content along two landscape transects. Journal of Hydrology 519, 1149-1161.
She, D., Qian, C., Timm, L.C., Beskow, S., Oliveira, L.M.D., 2017. Multi-scale correlations between soil hydraulic properties and associated factors along a Brazilian watershed transect. Geoderma 286, 15–24.
Shi, Z.H., Ai, L., Li, X., Huang, X.D., Wu, G.L., Liao, W., 2013. Partial least-squares regression for linking land-cover patterns to soil erosion and sediment yield in watersheds. Journal of Hydrology 498, 165–176.
Si, B.C., 2008. Spatial scaling analyses of soil physical properties: A review of spectral and wavelet methods. Vadose Zone Journal 7, 547–562.
Sok, T., Oeurng, C., Kaing, V., Sauvage, S., Sánchez-Pérez, J., 2021. Assessment of suspended sediment load variability in the Tonle Sap and Lower Mekong Rivers. Cambodia. Catena 202, 105291.
Starke, J., Ehlers, T.A., Schaller, M., 2020. Latitudinal effect of vegetation on erosion rates identified along western South America. Science 2020 (367), 1358–1361.
Syvitski, J., Vörösmarty, C., Kettner, A., Green, P., 2005. Impact of Humans on the Flux of Terrestrial Sediment to the Global Coastal Ocean. Science 308, 376–380.
Taesam, L., Ouarda, T., 2019. Multivariate nonstationary oscillation simulation of climate indices with empirical mode decomposition. Water Resources Research 55, 5033–5052.
Tong, X., Brandt, M., Yue, Y., Horion, S., Wang, K., Keersmaecker, W.D., Tian, F., Schurgers, G., Xiao, X., Luo, Y., 2018. Increased vegetation growth and carbon stock in China karst via ecological engineering. Nature Sustainability 1, 44–50.
Vercruysse, K., Grabowski, R.C., Rickson, R., 2017. Suspended sediment transport dynamics in rivers: multi-scale drivers of temporal variation. Earth-Science Reviews 166, 38–52.
Wang, T., Franz, T.E., Li, R., You, J., Shulski, M., Ray, C., 2017b. Evaluating climate and soil effects on regional soil moisture spatial variability using EOFs. Water Resources Research 53, 4022–4035.
Wang, S., Fu, B., Ciais, P., Piao, S., Wang, S., Feng, X., Wang, Y., Lü, Y., 2016. Reduced sediment transport in the Yellow River due to anthropogenic changes. Nature Geoscience 9, 38–41.
Wang, S., Fu, B., Liang, W., Liu, Y., Wang, Y., 2017a. Driving forces of changes in the water and sediment relationship in the Yellow River. Science of the Total Environment 576, 453–461.
Wang, K., Zhang, C., Chen, H., Yue, Y., Fu, Z., 2019. Karst landscapes of China: patterns, ecosystem processes and services. Landscape Ecology 34, 2743–2763.
Wen, X., Feng, Q., Deo, R.C., Wu, M., Yin, Z., Yang, L., Singh, V.P., 2019. Two-phase extreme learning machines integrated with the complete ensemble empirical mode decomposition with adaptive noise algorithm for multi-scale runoff prediction problems. Journal of Hydrology 570, 167–184.
Wilcox, B.P., Taucer, P.I., Munster, C.L., Owens, M.K., Mohanty, B.P., Sorenson, J.R., Bazan, R., 2008. Subsurface stormflow is important in semiarid karst shrublands. Geophysical Research Letters 35, L10403.
Wu, C., Yang, S., Lei, Y., 2012. Quantifying the anthropogenic and climatic impacts on water discharge and sediment load in the Pearl River (Zhujiang), China (1954–2009). Journal of Hydrology 452, 190–204.
Yang, Y., Jia, X., Wendroth, O., Liu, B., Shi, Y., Huang, T., Bai, X., 2019a. Noise-assisted multivariate empirical mode decomposition of saturated hydraulic conductivity along a south-north transect across the Loess Plateau of China. Soil Science Society of America Journal 83, 311–323.
Yang, Y., Wendroth, O., Kreba, S., Liu, B., 2019b. Estimating near-saturated soil hydraulic conductivity based on its scale-dependent relationships with soil properties. Vadose Zone Journal 18.
Yang, Y., Xintong, W., Tao, H., Ying, W., Wendroth, O., Chen, X., Liu, B., Zhang, G., 2022. Factors controlling saturated hydraulic conductivity along a typical black soil slope. Soil and Tillage Research 220, 105391.
Zhang, Z., Chen, X., Cheng, Q., Soulsby, C., 2019. Storage dynamics, hydrological connectivity and flux ages in a karst catchment: conceptual modelling using stable isotopes. Hydrology & Earth System Sciences 23, 51–71.
Zhang, B., He, C., Burnham, M., Zhang, L., 2016. Evaluating the coupling effects of climate aridity and vegetation restoration on soil erosion over the Loess Plateau in China. Science of the Total Environment 539, 436–449.
Zhang, Y., Long, Y., Zhang, X., Pei, Z., Lu, X., Wu, Z., Xu, M., Yang, H., Cheng, P., 2020b. Using depression deposits to reconstruct human impact on sediment yields from a small karst catchment over the past 600 years. Geoderma 363, 114168.
Zhang, F., Shi, X., Zeng, C., Wang, L., Xiao, X., Wang, G., Chen, Y., Zhang, H., Lu, X., Immerzeel, W., 2020a. Recent stepwise sediment flux increase with climate change in the Tuotuo River in the central Tibetan Plateau. Science Bulletin 65, 410–418.

Zhang, Q., Xu, C.Y., Singh, V.P., Yang, T., 2009. Multiscale variability of sediment load and streamflow of the lower Yangtze River basin: Possible causes and implications. Journal of Hydrology 368, 96–104.
Zhao, X., Lv, H., Lv, S., Sang, Y., Wei, Y., Zhu, X., 2021. Enhancing robustness of monthly streamflow forecasting model using gated recurrent unit based on improved grey wolf optimizer. Journal of Hydrology 601, 126607.
Zhao, Y., Zou, X., Liu, Q., Yao, Y., Li, Y., Wu, X., Wang, C., Yu, W., Wang, T., 2017. Assessing natural and anthropogenic influences on water discharge and sediment load in the Yangtze River, China. Science of The Total Environment 607, 920–932.
Zhao, Y., Wang, Y., Zhang, X., Li, W., 2018. Exploring scale-specific controls on soil water content across a 500-Kilometer transect using multivariate empirical mode decomposition. Vadose Zone Journal 17, 180097.
Zheng, H., Miao, C., Jiao, J., Borthwick, A., 2021. Complex relationships 1 between water discharge and sediment concentration across the Loess Plateau. China. Journal of Hydrology 126078.
Zhou, P., Luukkanen, O., Tokola, T., Nieminen, J., 2008. Effect of vegetation cover on soil erosion in a mountainous watershed. Catena 75, 319–325.
Zhu, X., Liang, Y., Tian, Z., Wang, X., 2021. Analysis of scale-specific factors controlling soil erodibility in southeastern China using multivariate empirical mode decomposition. Catena 199, 105131.